JOURNAL OF GUIDANCE, CONTROL, AND DYNAMICS
Vol. 21, No. 2, March–April 1998

Missile Autopilot Designs Using $\mathcal{H}_\infty$ Control with Gain Scheduling and Dynamic Inversion

Corey Schumacher* and Pramod P. Khargonekar†
University of Michigan, Ann Arbor, Michigan 48109-2122

Two nonlinear controller designs are presented for a bank-to-turn, air-to-air missile. The first controller is a gain-scheduled $\mathcal{H}_\infty$ design, and the second is a nonlinear dynamic inversion design using a two-timescale separation. We carried out a number of time- and frequency-domain analysis procedures on the resulting designs and tested their performance on a nonlinear simulation of the missile. We compared the controller designs for nominal performance, robustness to uncertainties in the aerodynamic coefficients, and sensitivity to measurement noise. The dynamic inversion controller was found to be significantly less robust to aerodynamic uncertainty. Using a μ-analysis test on a linearization of the closed-loop dynamics with the dynamic inversion controller, we were able to find a destabilizing aerodynamic uncertainty for the full nonlinear system.

Nomenclature

g	= acceleration due to gravity
I_{xx}, I_{yy}, I_{zz}	= moments of inertia about body axes x, y, and z
I_{xz}	= product of inertia about body axes x and z
L, M, N	= aerodynamic rolling, pitching, and yawing moments
p, q, r	= roll, pitch, and yaw rates about the body axes
T	= engine thrust force (along the missile body x axis)
V	= missile speed
X, Y, Z	= aerodynamic forces along the body axes x, y, and z
α	= angle of attack
β	= sideslip angle
ϕ, θ, ψ	= missile bank (roll) angle, pitch attitude angle, and heading angle

I. Introduction

THE aim of this paper is to present the main results from our recent study on the design of nonlinear controllers for a missile control problem. The missile control problem under investigation concerns postboost maneuvering of a bank-to-turn missile. This problem involves a fairly large change in the angle of attack, from 0 to 24 deg. This results in large changes in the dynamics of the missile. For example, the linearized dynamics go from being stable to unstable to stable again. Thus, the associated control problem involves dealing with significant nonlinear dynamics.

We chose to investigate two very different methodologies for this nonlinear control design problem: 1) gain scheduling of linear $\mathcal{H}_\infty$ designs and 2) nonlinear dynamic inversion. Although the design methodologies are substantially different, they aim to solve the same underlying control problem: robust control of nonlinear dynamical systems. There is a substantial body of literature on both of these methodologies. Although we will present the key features of these methodologies, the interested reader is referred to Refs. 1–7 for the gain scheduling approach and to Refs. 8–10 for the nonlinear dynamic inversion approach.

The paper begins with a discussion of the nonlinear missile model used in this study. The equations of motion for this model are taken from Ref. 11. Another reference for missile modeling is Ref. 12. Major features of the missile model and the objectives of the controller design are discussed in Sec. II. The nonlinear model equations of the missile are used to set a nonlinear dynamic simulation, which is used for carrying out all control analysis and design. In Secs. III and IV, we present a gain-scheduled $\mathcal{H}_\infty$-based controller with $\mathcal{D}$-implementation and then a dynamic inversion controller using a two-timescale separation. We carried out a number of time- and frequency-domain analysis procedures on the resulting designs. This analysis is presented in Sec. V.

The gain scheduling with linear $\mathcal{H}_\infty$ designs and the nonlinear dynamic inversion lead to similar nominal performance. This is interesting in that, given that the dynamics are highly nonlinear, it might be expected that nonlinear dynamic inversion would outperform the gain-scheduled design. Both methods do have advantages and disadvantages. A major advantage of the nonlinear dynamic inversion is that the controller design explicitly uses the nonlinear model and, thus, avoids having to design and interpolate linear controllers. On the other hand, it also leads to the main drawback of the nonlinear dynamic inversion approach, which is that a complete and accurate nonlinear model is necessary. The dynamic inversion controller is more sensitive to uncertainties in the aerodynamic coefficients and to measurement noise. The gain-scheduling approach also allows one to use the advanced linear robust control analysis and design techniques. The main disadvantage of the gain-scheduling approach is that the resulting nonlinear controller may not perform well against fast nonlinear dynamics. However, in this missile control design problem, we did not find this limitation. See Sec. V for a more detailed discussion of the relative advantages and disadvantages of these design techniques in the context of this missile control design problem.

II. Model and Control Objectives

The HaveDash II is an air-breathing, nonaxisymmetric airframe that is flown in a bank-to-turn (BTT) mode. In the air-to-air intercept problem, the guidance law produces acceleration commands in the body y and z axes based on estimates of the target motion. These acceleration commands can be converted into commands in roll angle and angle of attack, which are fed into the autopilot. Therefore, the primary variables of interest for controlling the missile's flight are angle of attack α and bank angle ϕ. The HaveDash missile was flown in flight tests with an angle-of-attack autopilot. The reader is referred to Refs. 9, 13, and 14 for treatment of autopilots that control angle of attack.

A. Missile Model

The missile model used in this study was a full nonlinear dynamic model using aerodynamic data for an air-to-air missile. The controller design study was performed for the missile flying at an altitude of 40,000 ft with a velocity of 1936 ft/s (Mach 2) and with the missile, having burned out its fuel, weighing 312 lb.

Received Oct. 7, 1996; revision received Aug. 8, 1997; accepted for publication Aug. 15, 1997.

*Graduate Student, Department of Aerospace Engineering; currently Research Aerospace Engineer, Flight Dynamics Directorate, U.S. Air Force Research Laboratory, Wright-Patterson Air Force Base, OH 45433-7531. E-mail: coreys@falcon.flight.wpafb.af.mil.

†Professor, Department of Electrical Engineering and Computer Science. E-mail: pramod@eecs.umich.edu.

The complete nonlinear rigid-body equations of motion are used to derive the missile model. The derivation of these equations can be found in Ref. 11. The rigid-body, nonlinear equations of motion for an aircraft with constant mass are

$$\dot{\phi} = p + (q\sin\phi + r\cos\phi)\tan\theta \tag{1}$$

$$\dot{\theta} = q\cos\phi - r\sin\phi \tag{2}$$

$$\dot{\psi} = \frac{q\sin\phi + r\cos\phi}{\cos\theta} \tag{3}$$

$$\begin{aligned}\dot{V} = {} & [(T+X)/m]\cos\alpha\cos\beta + (Y/m)\sin\beta \\ & + (Z/m)\sin\alpha\cos\beta + g(-\sin\theta\cos\alpha\cos\beta \\ & + \cos\theta\sin\phi\sin\beta + \cos\theta\cos\phi\sin\alpha\cos\beta)\end{aligned} \tag{4}$$

$$\begin{aligned}\dot{\alpha} = {} & -\frac{T+X}{mV\cos\beta}\sin\alpha + \frac{Z\cos\alpha}{mV\cos\beta} + q - (p\cos\alpha \\ & + r\sin\alpha)\tan\beta + \frac{g}{V\cos\beta}\cos\alpha\cos\phi\cos\theta\sin\alpha\sin\theta\end{aligned} \tag{5}$$

$$\begin{aligned}\dot{\beta} = {} & -(r\cos\alpha - p\sin\alpha) - \frac{T+X}{mV}\cos\alpha\sin\beta \\ & + \frac{Y\cos\beta}{mV} - \frac{Z}{mV}\sin\alpha\sin\beta + \frac{g}{V}(\cos\theta\sin\phi\cos\beta \\ & + \sin\theta\cos\alpha\sin\beta - \cos\theta\cos\phi\sin\alpha\sin\beta)\end{aligned} \tag{6}$$

$$\dot{p} = I_{ppq}pq + I_{pqr}qr + I_{pl}L + I_{pn}N \tag{7}$$

$$\dot{q} = I_{qpp}p^2 + I_{qrr}r^2 + I_{qpr}pr + I_{qm}M \tag{8}$$

$$\dot{r} = I_{rpq}pq + I_{rqr}qr + I_{rl}L + I_{rn}N \tag{9}$$

These equations of motion can be summarized as $\dot{\boldsymbol{x}} = f(\boldsymbol{x}, \boldsymbol{u})$ with $\boldsymbol{x} := (\alpha, \beta, p, q, r, \phi, \theta, \psi, V)^T$ and $\boldsymbol{u} := (\delta e, \delta a, \delta r)$. The forces and moments are also dependent on the altitude of the missile. The values for the moments of inertia can be found in Table 1, with the numerical values in slug · feet squared.

The model includes tables containing the forces and moments acting on the missile as functions of angle of attack, sideslip angle, Mach number, control surface deflections, and altitude (gravity and air density changes). The data used in this study can be found in Ref. 15. The HaveDash II missile has four control surfaces, but they do not move independently. Fin mixing logic is used to calculate effective elevator (δe), aileron (δa), and rudder (δr) deflections from the fin positions. The aerodynamic data for the missile are given using δe, δa, and δr as the control deflections. Thus, there are in effect three control surfaces available for the control of the missile dynamics. Second-order actuator models with rate and deflection saturation are included in the nonlinear model.

Table 1 Moments of inertia

$I_{xxzzxz2} = I_{xx}I_{zz} - I_{xz}^2 = 105.64$	$I_{pn} = \dfrac{I_{xz}}{I_{xxzzxz2}} = 0.0025$
$I_{qm} = \dfrac{1.0}{I_{yy}} = 0.0104$	$I_{rl} = \dfrac{I_{xz}}{I_{xxzzxz2}} = 0.0025$
$I_{rn} = \dfrac{I_{xx}}{I_{xxzzxz2}} = 0.0104$	$I_{ppq} = I_{xz}\dfrac{I_{zz} + I_{xx} - I_{yy}}{I_{xxzzxz2}} = 0.003$
$I_{pqr} = \dfrac{I_{zz}(I_{yy} - I_{zz}) - I_{xz}^2}{I_{xxzzxz2}} = -0.092$	$I_{rqr} = \dfrac{I_{xz}(I_{yy} - I_{zz}) - I_{xx}I_{xz}}{I_{xxzzxz2}} = -0.003$
$I_{rpq} = \dfrac{I_{xx}(I_{xx} - I_{yy}) + I_{xz}^2}{I_{xxzzxz2}} = -0.988$	$I_{qpp} = \dfrac{-I_{xz}}{I_{yy}} = -0.0027$
$I_{qrr} = \dfrac{I_{xz}}{I_{yy}} = 0.0027$	$I_{qpr} = \dfrac{I_{zz} - I_{xx}}{I_{yy}} = 0.990$

The dynamics of the missile change dramatically with variations in angle of attack. At low α, it is very easy to roll the missile rapidly, with little effect on other states. However, at higher α, there is large coupling between sideslip angle and roll rate. This is due to the $p\sin\alpha$ term in Eq. (6). The missile aerodynamic coefficients also vary substantially with angle of attack. The missile dynamics are naturally unstable in the vicinity of 10-deg angle of attack but stable both above and below the unstable region. These variations in dynamics require a nonlinear controller to control the missile over the entire range of angle of attack.

B. Control Objectives

The controller must satisfy the following requirements. It must achieve an angle-of-attack command response with zero steady-state error and a time constant of less than 0.3 s over a range of 0–24-deg angle of attack. It must achieve a roll-angle command response with zero steady-state error over a range of ±180 deg. The controller must keep sideslip angle less than 5 deg for all maneuvers. This objective is assumed by most BTT logic and is a requirement for the air-breathing propulsion system of the HaveDash missile. The open-loop gain from control deflections to control deflection commands should be less than −25 dB at 400 rad/s for the elevator and rudder deflection commands and less than −25 dB at 500 rad/s for the aileron deflection command. This control attenuation is necessary to ensure robust stability to flexure dynamics, which is not included in the nonlinear model. This requirement is discussed in Ref. 16. Because of actuator hardware limits, the controller should use actuator deflections less than 30 deg and actuator rates less than 573 deg/s. These limits were particularly restrictive for the dynamic inversion controller, which tended to use larger, faster control deflections. The controller should also achieve robustness to variations in aerodynamic coefficients of up to 20%. This level of uncertainty was chosen as being typical of the level of uncertainty in aerodynamic coefficients.

III. Controller Design with $\mathcal{H}_\infty$ Synthesis, Gain Scheduling, and $\mathcal{D}$ Implementation

We designed a nonlinear controller for the missile using a series of linear $\mathcal{H}_\infty$ full state feedback controllers with $\mathcal{D}$-implementation gain scheduling to cover the desired portion of the flight envelope.

A. Linear Controller Design with $\mathcal{H}_\infty$ Synthesis

Linear controllers were designed for a series of linear models taken from the simulation with the missile flying at a speed of 1936 ft/s, an altitude of 40,000 ft, and angles of attack of α = 1, 5, 10, 13, 15, 17, 20, and 23 deg. These angles of attack were chosen to capture the essential features of the aerodynamics of the missile. For example, the natural frequency of the linearized lateral dynamics increased from 10 to 17 deg α but then decreased as α increased further. Therefore, we chose $\alpha = 17$ deg as a design point for a linear $\mathcal{H}_\infty$ controller. The linear controller design methodology used in this paper is similar to that in Ref. 17. The first step is to create a synthesis model.

1. *Developing the Synthesis Model*

The synthesis model used in the $\mathcal{H}_\infty$ controller design process is shown in Fig. 1. The synthesis model is composed of the linear model of the missile dynamics, with weights added to create the outputs z. The weights became the design knobs that are tuned to achieve the desired performance.

The signal $\boldsymbol{w}_1$ represented the commanded inputs. The vectors $\boldsymbol{z}^1, \boldsymbol{z}^2, \boldsymbol{z}^3$, and $\boldsymbol{z}^4$ contain the signals that are weighted in the $\mathcal{H}_\infty$ design process. Note that the signals $\boldsymbol{z}^3$ are calculated using the system model. In particular, they are not derivatives of the measured state variables. The signal $\boldsymbol{z}^4$ represented the control inputs to the system: the elevator command δe_c, the aileron command δa_c, and the rudder command δr_c. Because zero steady-state error to a step command was required for α and p commands, two integrators were added to W_1. The matrices W_2, W_3, and W_4 are simply diagonal matrices and do not contain any dynamics. The vector $\boldsymbol{y}$ consists of the states of the plant as well as the outputs of the error integrators

Table 2 Linear controller design information, $\alpha = 15$ deg

Linear model

$$A = \begin{pmatrix} -0.89 & 0 & 0 & 1 & 0 & 0 & 0 \\ 0 & -0.13 & -0.26 & 0 & -0.97 & 0 & 0 \\ 0 & -2806 & 0 & 0 & 0 & 0 & 0 \\ -72.7 & 0 & 0 & 0 & 0 & 0 & 0 \\ 0 & -24.4 & 0 & 0 & 0 & 0 & 0 \\ 1 & 0 & 0 & 0 & 0 & 0 & 0 \\ 0 & 0 & 1 & 0 & 0 & 0 & 0 \end{pmatrix} \quad B = \begin{pmatrix} -0.145 & -0.028 & 0 \\ 0 & 0.032 & 0.080 \\ 0 & -1382 & -95.2 \\ -121.7 & -24.1 & 0 \\ 0 & -27.4 & -67.2 \\ 0 & 0 & 0 \\ 0 & 0 & 0 \end{pmatrix}$$

Design weights

$c_1 = 8$ $c_2 = 7$ $c_3 = 9$ $c_4 = 0.1$ $c_5 = 0$ $c_6 = 0.25$ $c_7 = 0$
$c_8 = 0.03$ $c_9 = 0$ $c_{10} = 0$ $c_{11} = 3$ $c_{12} = 6$ $c_{13} = 3$ $\gamma = 2.55$

Linear controller gains

$$K = \begin{pmatrix} 1.129 & 0.372 & -0.000 & 0.181 & -0.007 & 8.637 & -0.019 \\ 0.002 & -1.654 & 0.018 & 0.001 & -0.025 & 0.028 & 0.134 \\ -0.021 & -4.451 & -0.021 & -0.006 & 0.333 & -0.306 & 0.516 \end{pmatrix}$$

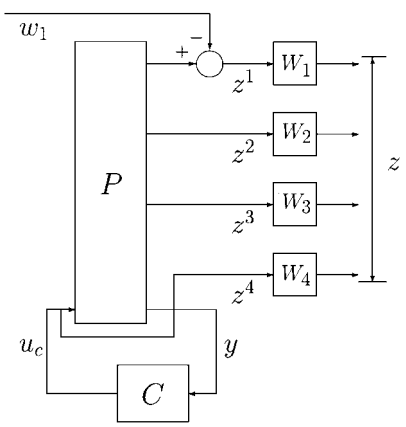

Fig. 1 $\mathcal{H}_\infty$ controller synthesis model: $w_1 = (\alpha_{cmd}\ p_{cmd})^T$; $z^1 = (\alpha - \alpha_{cmd}\ p - p_{cmd})^T$; $z^2 = (\beta\ q\ r)^T$; $z^3 = (\dot{\alpha}\ \dot{\beta}\ \dot{p}\ \dot{q}\ \dot{r})^T$; $z^4 = (\delta e_c\ \delta a_c\ \delta r_c)^T$; $W_1 = \text{diag}(c_i/s), i = 1, \ldots, 2$; $W_2 = \text{diag}(c_i), i = 3, \ldots, 5$; $W_3 = \text{diag}(c_i), i = 6, \ldots, 10$; $W_4 = \text{diag}(c_i), i = 11, \ldots, 13$; and $y = (\dot{\alpha}\ \dot{\beta}\ \dot{p}\ \dot{q}\ \dot{r}\ \alpha_e/s\ p_e/s)^T$.

in W_1. This signal is fed back to the controller to generate the control inputs u_c.

As an example, the data for the design of the $\mathcal{H}_\infty$ controller for the linear model at $\alpha = 15$ deg are given in Table 2. Information on the other linear designs can be found in Ref. 15. The states for the linear model are $\boldsymbol{x} = (\alpha, \beta, p, q, r, \int(\alpha_e), \int(p_e))^T$. The states are assumed available for feedback but in practice must be estimated using accelerometer and rate gyro measurements. The control inputs are $\boldsymbol{u} = (\delta e, \delta a, \delta r)^T$. The $\mathcal{H}_\infty$ controllers for each linear model were calculated using the hinffi command from MatLab.

2. Choice of Design Weights

The final design weights for each linear controller are chosen via an iterative process. First, initial choices of weights were made and the resulting controller examined. If the Bode response plots are unacceptable due to excessive control usage, slow speed of response, excessive longitudinal/lateral coupling, inadequate damping, or a variety of other reasons, the appropriate weights are adjusted and the new controller examined. If the weights are adjusted systematically, the process is not difficult or time consuming. A detailed discussion of the application of this type of procedure to an aircraft control problem can be found in Ref. 17.

The selection of the exact weights is heavily influenced by the nominal performance objectives. The weights c_1 and c_2 were chosen to give fast response to α and p commands, whereas c_3 was made large to weight sideslip angle heavily and reduce β during a maneuver. The weights on state derivatives and c_4 were adjusted to achieve the desired damping. Adjusting the control weights c_{11}–c_{13} changed the control attenuation. There is coupling between the effects of all of the weights, and a number of iterations were necessary to meet all requirements satisfactorily. In general, the weights were chosen to maximize response speeds while achieving damping ratios of at least 0.6 and meeting the control attenuation requirements. Some aspects of performance, such as sideslip attenuation, required evaluation on the nonlinear simulation.

B. Gain Scheduling and $\mathcal{D}$ Implementation

The set of linear controllers were gain scheduled using cubic spline interpolation and implemented using $\mathcal{D}$ implementation to provide a nonlinear controller for the missile model over a range of $\alpha = 0$–24 deg. The angles of attack at which linear controllers were designed were chosen in two steps. First, linear models were developed over the range of 0–24-deg angle of attack and examined to determine where substantial changes took place. Then, linear controllers were designed near the endpoints of the α range and whenever the dynamics had changed enough to degrade performance using the nearest controllers. Recall that linear controllers were designed at $\alpha = 1$, 5, 10, 13, 15, 17, 20, and 23 deg. The function $K(\alpha)$ in Fig. 2 is a cubic spline interpolation across these eight linear controllers to determine the appropriate control gains based on the present angle of attack.

The complete controller architecture is shown in Fig. 2. The command conversion logic, which changes the ϕ_c to a p_c, was designed to meet a number of overall design objectives. The gain K_ϕ converts the ϕ_c to a (saturation-limited) wind-axis roll rate command, which is finally converted to a body-axis roll rate command. The value of K_ϕ was chosen from tests conducted on the nonlinear simulation. The value $K_\phi = 4$ was found to give the best overall performance for a range of α and ϕ commands.

For the $\mathcal{D}$-implementation gain-scheduled controller, the integrators on the command-following errors are pulled through to the back side of the controller, and the state rates and command-following errors are inputs to the controller, instead of the states and the integrals of the command-following errors. The state measurements could be smoothed and then differentiated. In the simulation results of Sec. V, the actual values of the derivatives were used to calculate the control, except in the test of sensitivity to noise in Sec. V.D. In that case, inaccurate values of the derivatives calculated from the noisy measurements were used. Furthermore, in the digital implementation, the derivative simply becomes the difference between the states at two time points. An important consequence of the $\mathcal{D}$ implementation is that the controller does not need to refer to a nominal design point, as the controller takes the change in state values as inputs, instead of the state values themselves. A detailed discussion of the $\mathcal{D}$-implementation gain scheduling that addresses these issues can be found in Ref. 1.

There is one difference between the result given in Ref. 1 and the $\mathcal{D}$ implementation used here. In Ref. 1, it is required that the number of control commands and, hence, the number of integrators in the controller be equal to the number of independent control inputs. In our controller, there are two reference commands, two

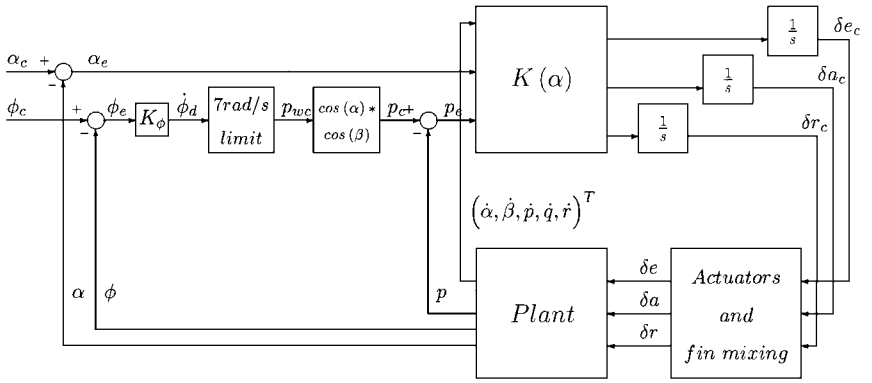

Fig. 2 $\mathcal{D}$-implementation gain-scheduled $\mathcal{H}_\infty$ controller structure. Note: $K_\phi = 4$.

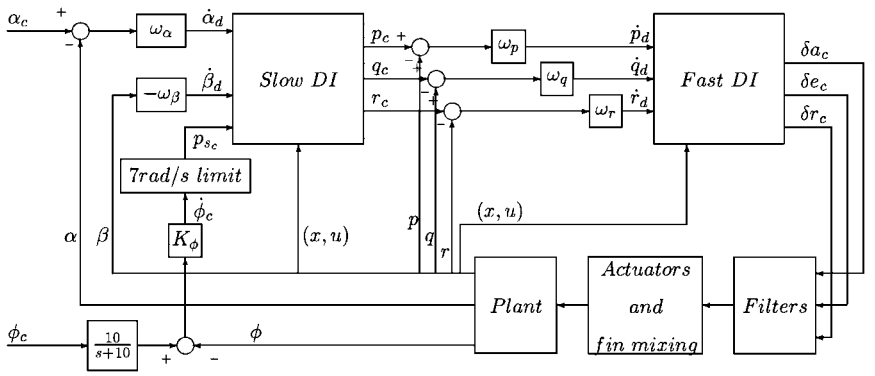

Fig. 3 Dynamic inversion controller structure.

integrators, and three control commands. When the two integrators are pulled through the controller $K(\alpha)$, a third integrator appears. This adds one state to the controller that was not there without the $\mathcal{D}$ implementation. However, this causes no difficulty because this extra state, which has a zero eigenvalue in the closed-loop system, is a part of the controller and is not a physical eigenvalue. In this situation, the eigenvalues of the linearized, closed-loop system are exactly those designed for by the linear controller, with the addition of a zero eigenvalue in a controller state.

IV. Nonlinear Dynamic Inversion Controller

The second design methodology used is a dynamic inversion approach using a two-timescale assumption to separate the dynamics. Another example of this method can be found in Ref. 10. The controller structure is shown in Fig. 3.

A. Dynamic Inversion: Inner Control Loop for the Fast States

The inner loop of the dynamic inversion control law controls the fast states p, q, and r. This loop calculates control surface deflection commands from the rate commands p_c, q_c, and r_c given by the slow inversion in Fig. 3, under the assumption that the slow variables α, β, and ϕ are constant during the maneuver. The desired dynamics used are given by $\dot{p}_d = \omega_p(p_c - p)$, $\dot{q}_d = \omega_q(q_c - q)$, and $\dot{r}_d = \omega_r(r_c - r)$, where $\omega_p = 30$ rad/s, $\omega_q = 18$ rad/s, and $\omega_r = 30$ rad/s. These values were chosen to be as large as possible without causing actuator saturation. The control deflection commands generated by the inner control loop are filtered to guarantee the necessary attenuation. Each control deflection command is sent through a low-pass filter to guarantee the necessary attenuation of control commands to avoid exciting structural modes. The filters used for the pitch and yaw channels were $6400/(s^2 + 160s + 6400)$, and the filter used for the roll channel was $10{,}000/(s^2 + 200s + 10{,}000)$.

The frequencies of these filters must be large enough that there is an adequate timescale separation between the filter dynamics and the desired dynamics for the inner-loop states p, q, and r to maintain the stability and performance of the closed-loop system. The necessary control attenuation instead could have been achieved by lowering the desired frequencies of the inner- and outer-loop dynamics. However, this method gave no direct control of control attenuation and required much slower desired dynamics to achieve the same control attenuation as was achieved with the filters.

For the purpose of the fast inversion, the aerodynamic moments L, M, and N in Eqs. (7–9) are assumed to be functions of δe, δa, and δr. Dimensional aerodynamic derivatives are calculated using a difference approximation about the present states and control positions so that the dependence of the moments on the control deflections can be isolated. Then, for small δe, δa, and δr

$$L = L_0 + L_{\delta e}\delta e + L_{\delta a}\delta a + L_{\delta r}\delta r \tag{10}$$

$$M = M_0 + M_{\delta e}\delta e + M_{\delta a}\delta a + M_{\delta r}\delta r \tag{11}$$

$$N = N_0 + N_{\delta e}\delta e + N_{\delta a}\delta a + N_{\delta r}\delta r \tag{12}$$

where L_0 is the roll moment due to the missile body and is a function of α, β, and Mach number; $L_{\delta a}$ is the roll moment generated per unit aileron deflection; and the other terms are similarly defined. Then, with the given substitutions, we have

$$\begin{bmatrix} \delta a_c \\ \delta e_c \\ \delta r_c \end{bmatrix} = [I] \begin{bmatrix} \dot{p}_d - (I_{ppq}pq + I_{pqr}qr + I_{pl}L_0 + I_{pn}N_0) \\ \dot{q}_d - \left(I_{qpp}p^2 + I_{qrr}r^2 + I_{qpr}pr + I_{qm}M_0\right) \\ \dot{r}_d - (I_{rpq}pq + I_{rqr}qr + I_{rl}L_0 + I_{rn}N_0) \end{bmatrix} \tag{13}$$

where

$$I = \begin{pmatrix} I_{pl}L_{\delta a} + I_{pn}N_{\delta a} & I_{pl}L_{\delta e} + I_{pn}N_{\delta e} & I_{pl}L_{\delta r} + I_{pn}N_{\delta r} \\ I_{qm}M_{\delta a} & I_{qm}M_{\delta e} & I_{qm}M_{\delta r} \\ I_{rl}L_{\delta a} + I_{rn}N_{\delta a} & I_{rl}L_{\delta e} + I_{rn}N_{\delta e} & I_{rl}L_{\delta r} + I_{rn}N_{\delta r} \end{pmatrix}^{-1}$$

B. Dynamic Inversion: Outer Control Loop for the Slow States

A second inversion is applied to the dynamics of the slow states α and β. The existing command logic used in the $\mathcal{H}_\infty$ controller is used to convert a roll angle command into a stability-axis roll rate command p_{s_c}, so that it is not necessary to invert the dynamics associated with the roll angle ϕ. The only significant change in this logic is the addition of a filter on ϕ_c so that the ϕ_c will not change too rapidly for the inner loop to follow. The slow inversion assumes that

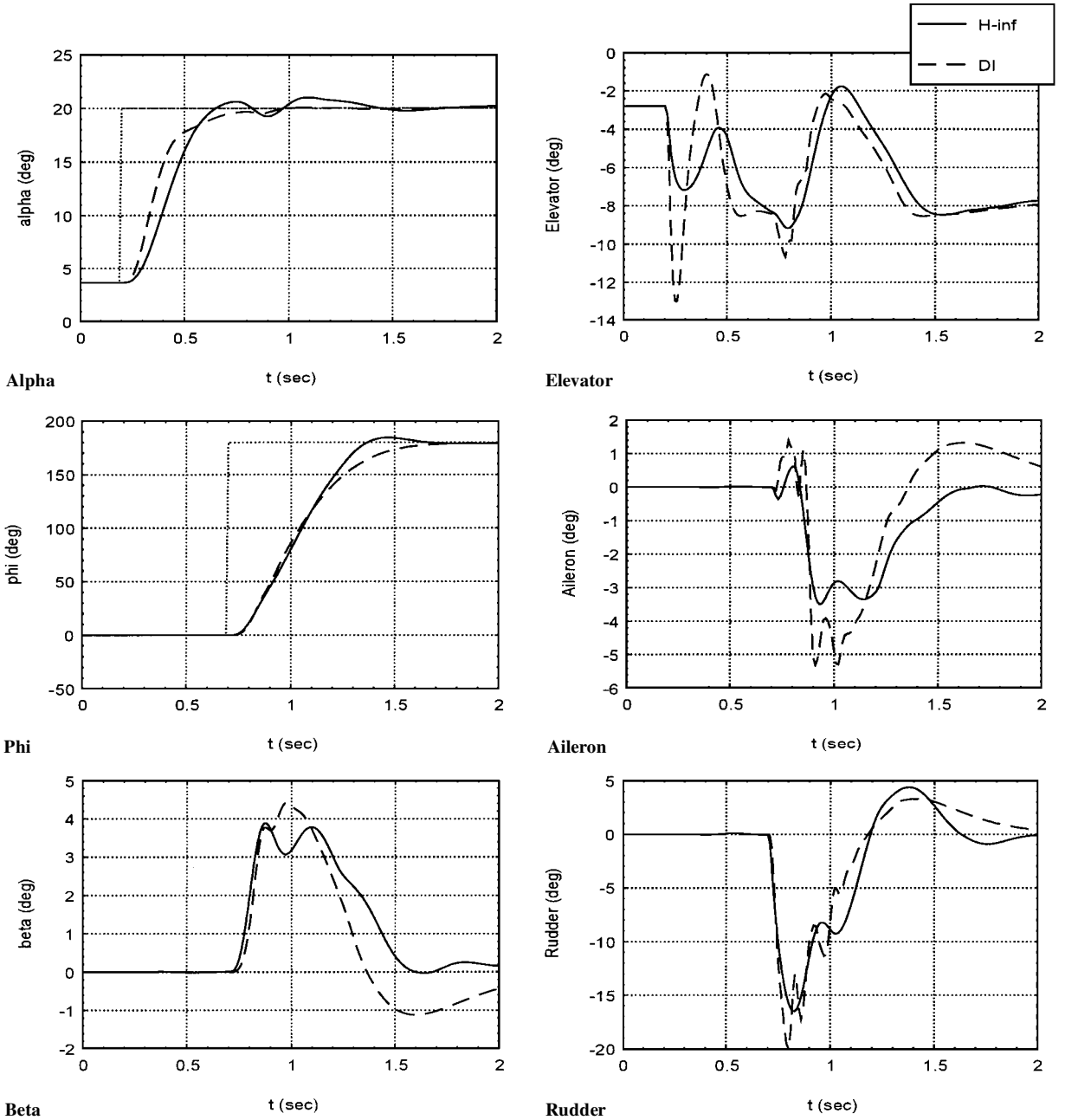

Alpha **Elevator**

Phi **Aileron**

Beta **Rudder**

Fig. 4 Nominal performance.

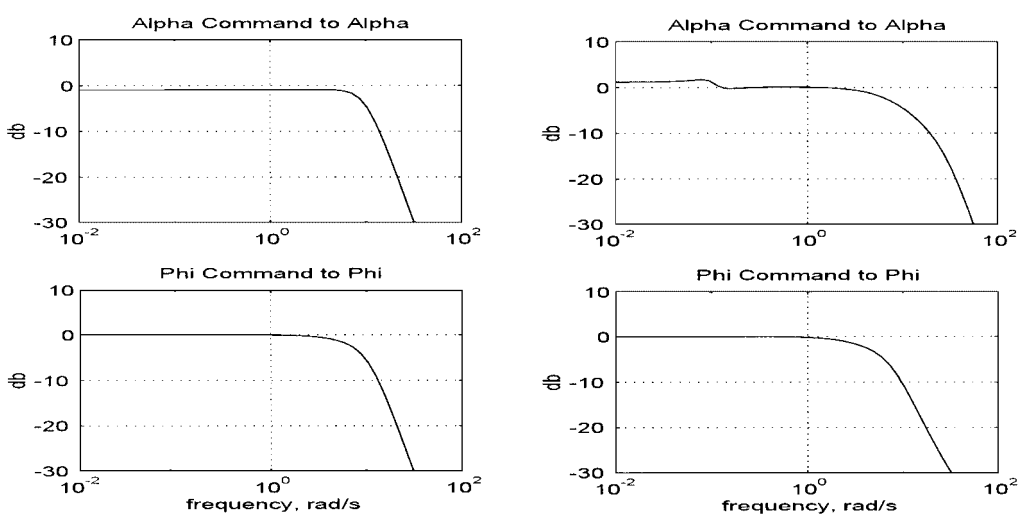

a) $\mathcal{H}_\infty$ controller **b) Dynamic inversion controller**

Fig. 5 Closed-loop frequency responses for the linearized systems.

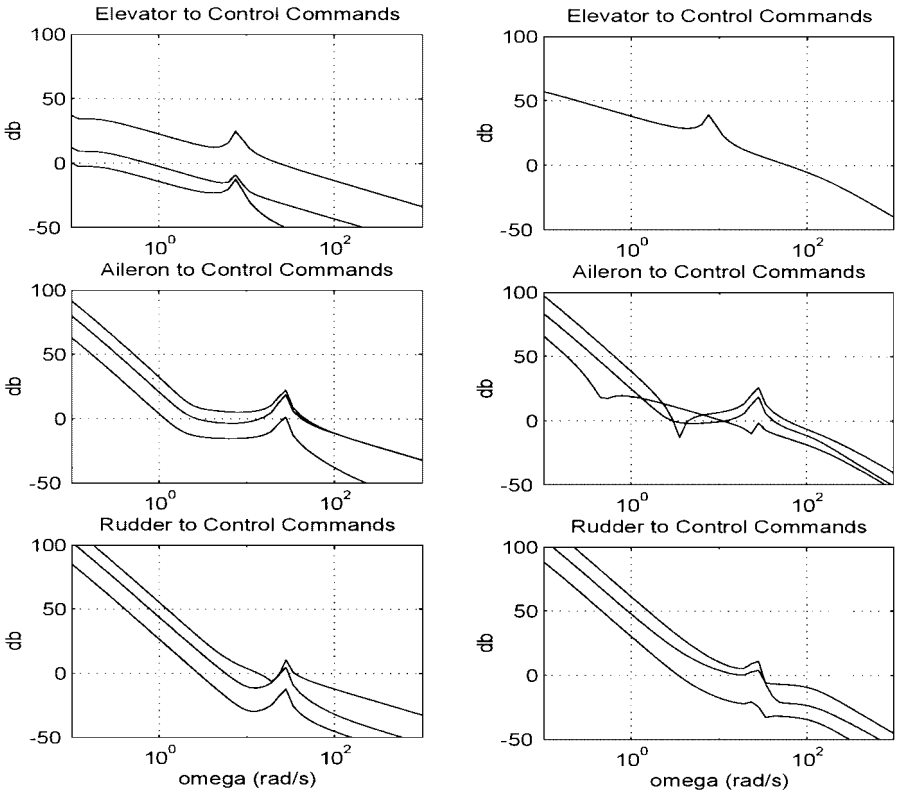

Fig. 6 Open-loop frequency responses for the linearized systems.

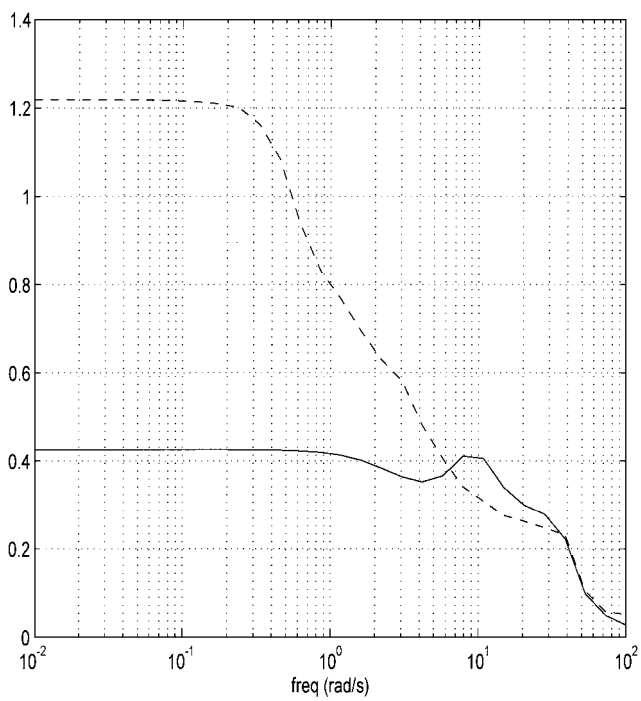

Fig. 7 Linearized closed-loop robust stability real μ: – – –, dynamic inversion controller and ——, $\mathcal{H}_\infty$ controller.

the fast states track their commanded values instantly, ignoring the effects of transient body rate dynamics. The slow inversion attempts to replace the actual α and β dynamics with the desired dynamics $\dot{\alpha}_d = \omega_\alpha(\alpha_c - \alpha)$ and $\dot{\beta}_d = -\omega_\beta \beta$, where $\omega_\alpha = 6$ rad/s and $\omega_\beta = 10$ rad/s. These frequencies have been chosen low enough to avoid coupling between the inner- and outer-loop dynamics.

The values of the desired frequencies were chosen to give the fastest possible command response while still keeping sideslip small. The desire to keep β small led directly to the large ω_β value. The need for a large frequency separation between the inner-loop and outer-loop dynamics imposed limits on the size of the outer-loop frequencies, inasmuch as the inner-loop frequencies were chosen to be as large as possible without causing actuator saturation.

With Eqs. (5) and (6) and the external inputs as described, the slow inversion control law has the form

$$q_c = \dot{\alpha}_d + p_{s_c}\tan\beta + \left(\frac{T+X}{mV\cos\beta}\sin\alpha - \frac{Z\cos\alpha}{mV\cos\beta} - \frac{g}{V\cos\beta}\cos\alpha\cos\phi\cos\theta + \sin\alpha\sin\theta\right) \tag{14}$$

$$p_c = p_{s_c}\cos\alpha + \left[\dot{\beta}_d + \frac{T+X}{mV}\cos\alpha\sin\beta - \frac{Y\cos\beta}{mV} + \frac{Z}{mV}\sin\alpha\sin\beta - \frac{g}{V}(\cos\theta\sin\phi\cos\beta + \sin\theta\cos\alpha\sin\beta - \cos\theta\cos\phi\sin\alpha\sin\beta)\right]\sin\alpha \tag{15}$$

$$r_c = p_{s_c}\sin\alpha - \left[\dot{\beta}_d + \frac{T+X}{mV}\cos\alpha\sin\beta - \frac{Y\cos\beta}{mV} + \frac{Z}{mV}\sin\alpha\sin\beta - \frac{g}{V}(\cos\theta\sin\phi\cos\beta + \sin\theta\cos\alpha\sin\beta - \cos\theta\cos\phi\sin\alpha\sin\beta)\right]\cos\alpha \tag{16}$$

A similar development can be found in Ref. 9.

V. Comparison of Designs

In this section, we discuss the advantages and disadvantages of the two controller designs considered. We first compare the performance of the two designs in areas such as speed of response, size of the control deflections used, and degree of coupling between input channels. The next step is to examine the robustness of the two

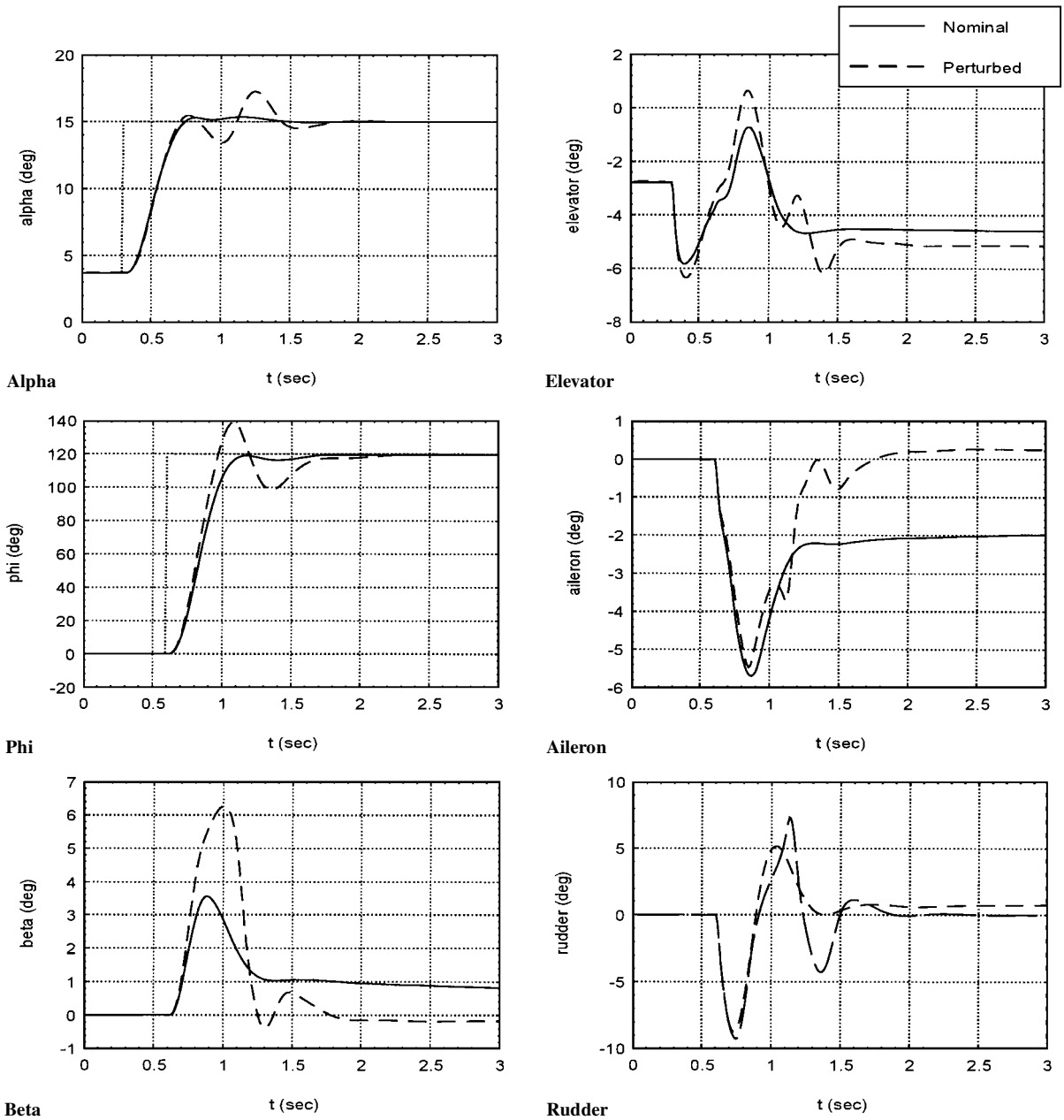

Fig. 8 $\mathcal{H}_\infty$ controller nominal and perturbed dynamics.

designs to uncertainty in the aerodynamic coefficients. Finally, we examine the sensitivity of the controllers to measurement noise.

A. Performance

The complete controllers were tested on the nonlinear simulation of the missile. Numerous tests over a variety of maneuvers were run to evaluate the stability and performance of the controllers. For the maneuvers shown, the simulation was initialized at $\alpha = 3.66$ deg with all control surfaces at their trim positions ($\delta e = 2.8$ deg, $\delta a = 0$, and $\delta r = 0$). This is not a true steady cruise condition because the missile is not thrusting. The missile speed decreases throughout the maneuver. The missile was flying at 40,000 ft with an initial velocity of 2086 ft/s (approximately Mach 2.2). The controller task was to track step commands in angle of attack α and roll angle ϕ, while avoiding actuator saturations and keeping sideslip small. In the figures in this section, commanded values are shown as dotted lines, the results for the gain-scheduled $\mathcal{H}_\infty$ controller are shown as solid lines, and the results for the dynamic inversion controller are shown as dashed lines.

The results for a test maneuver are shown in Fig. 4. This maneuver consists of a pitch up to $\alpha = 20$ deg and then a 180-deg roll. Because a large part of this maneuver occurs at high angle of attack, the missile velocity decreases substantially during the maneuver. The $\mathcal{H}_\infty$ controller was designed at Mach 2 (1936 ft/s) and is not gain scheduled with Mach number, so there is a small loss of performance due to the changed aerodynamic coefficients. The dynamic inversion controller uses full knowledge of the dynamic coefficients and, thus, has an advantage over the $\mathcal{H}_\infty$ controller.

The nominal performance of the two controllers is similar, with only small differences. Both controllers meet the basic performance specifications, with acceptable α and ϕ responses and the maximum sideslip angle achieved in each case near 4 deg. The $\mathcal{H}_\infty$ controller exhibits some overshoot in both the α- and ϕ-command responses, whereas the dynamic inversion controller does not. This is natural because the desired dynamics used for the dynamic inversion controller were first order. The dynamic inversion controller exhibits superior decoupling between pitch and roll commands. This is most clearly seen in the $\mathcal{H}_\infty$ controller's angle-of-attack response during the roll portion of the maneuver. The dynamic inversion controller achieves this decoupling at the cost of larger, faster control deflections.

B. Linearization and Robustness of the Closed-Loop Systems

To further examine the performance of the two controllers, we linearized the dynamics of the plant with each controller. This was done for both the closed-loop dynamics from α and ϕ commands

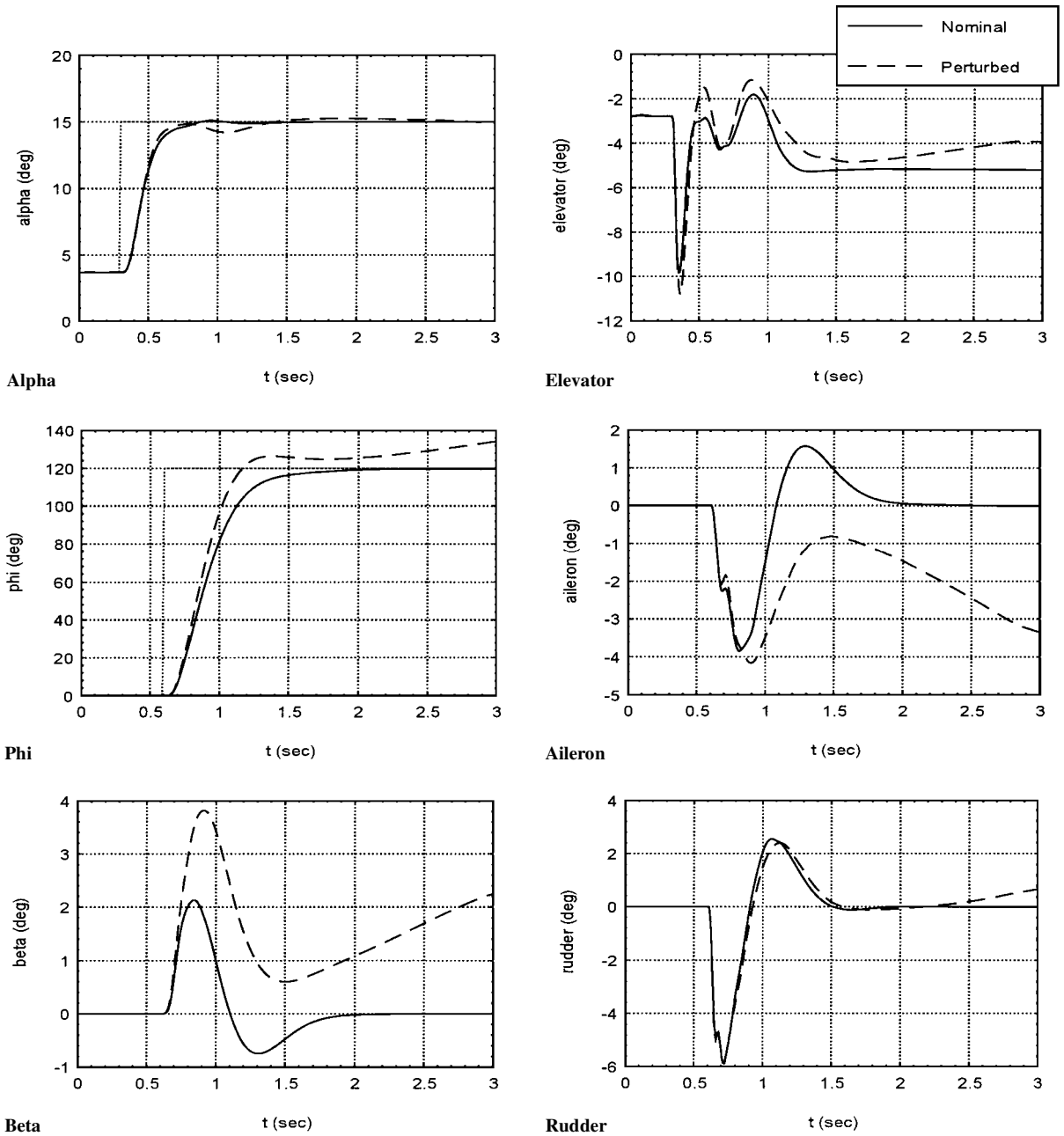

Fig. 9 Dynamic inversion controller nominal and perturbed dynamics.

to α and ϕ and the open-loop dynamics from control deflections to control deflection commands. Figures 5 and 6 show frequency response plots for both controllers linearized at $\alpha = 15$ deg. The frequency responses for the dynamic inversion controller are very similar throughout the α range, although there is more variation with the $\mathcal{H}_\infty$ controller because the gain-scheduled linear controllers are different. The selected flight condition is typical of the frequency responses at other angles of attack, with only small differences. There is only one line on the upper plot of Fig. 6b because the other two responses, showing coupling between elevator and aileron/rudder commands, had magnitude less than 50 dB over the frequency range of the plots.

Figures 5a and 6a show the responses for the $\mathcal{H}_\infty$ controller, and Figs. 5b and 6b show the responses for the dynamic inversion controller. The $\mathcal{H}_\infty$ controller exhibits higher bandwidths for α and ϕ commands, which is consistent with the faster response times seen in the preceding section. Both controllers exhibit the necessary attenuation of control deflection commands to prevent excitation of the body bending modes. In the case of the dynamic inversion controller, this was forced by the use of the second-order filters on the control commands. This gives the dynamic inversion controller a higher crossover frequency because the broken-loop frequency response plots roll off at an additional -40 dB/decade after the filters become effective, and the $\mathcal{H}_\infty$ controller responses only roll off at -20 dB/decade. Because of the faster rolloff, the dynamic inversion controller is able to have higher crossover frequencies. This was seen in the control deflection plots of Fig. 4 and is partly responsible for the tighter command following and reduced coupling shown by the dynamic inversion controller.

The first step in our robustness analysis was to perform μ-analysis tests on the linearizations of the closed-loop systems just discussed. The real-μ plots shown in Fig. 7 are for 20% uncertainties in the 13 largest coefficients of the linear models that affect the dynamics of the primary states α, β, p, q, and r. These coefficients correspond to the $a11$, $a41$, $a22$, $a32$, $a52$, $b11$, $b41$, $b32$, $b42$, $b52$, $b23$, $b33$, and $b53$ elements of the linear models given in Table 2.

The μ-analysis tests were performed using the MatLab μ-tools toolbox. For the $\mathcal{H}_\infty$ controller, the peak of the μ plot is at 0.425, indicating stability robustness to 47% uncertainties in the aerodynamic coefficients. For the dynamic inversion controller, however, the peak is at 1.22, indicating stability robustness only to 16% uncertainties in the coefficients.

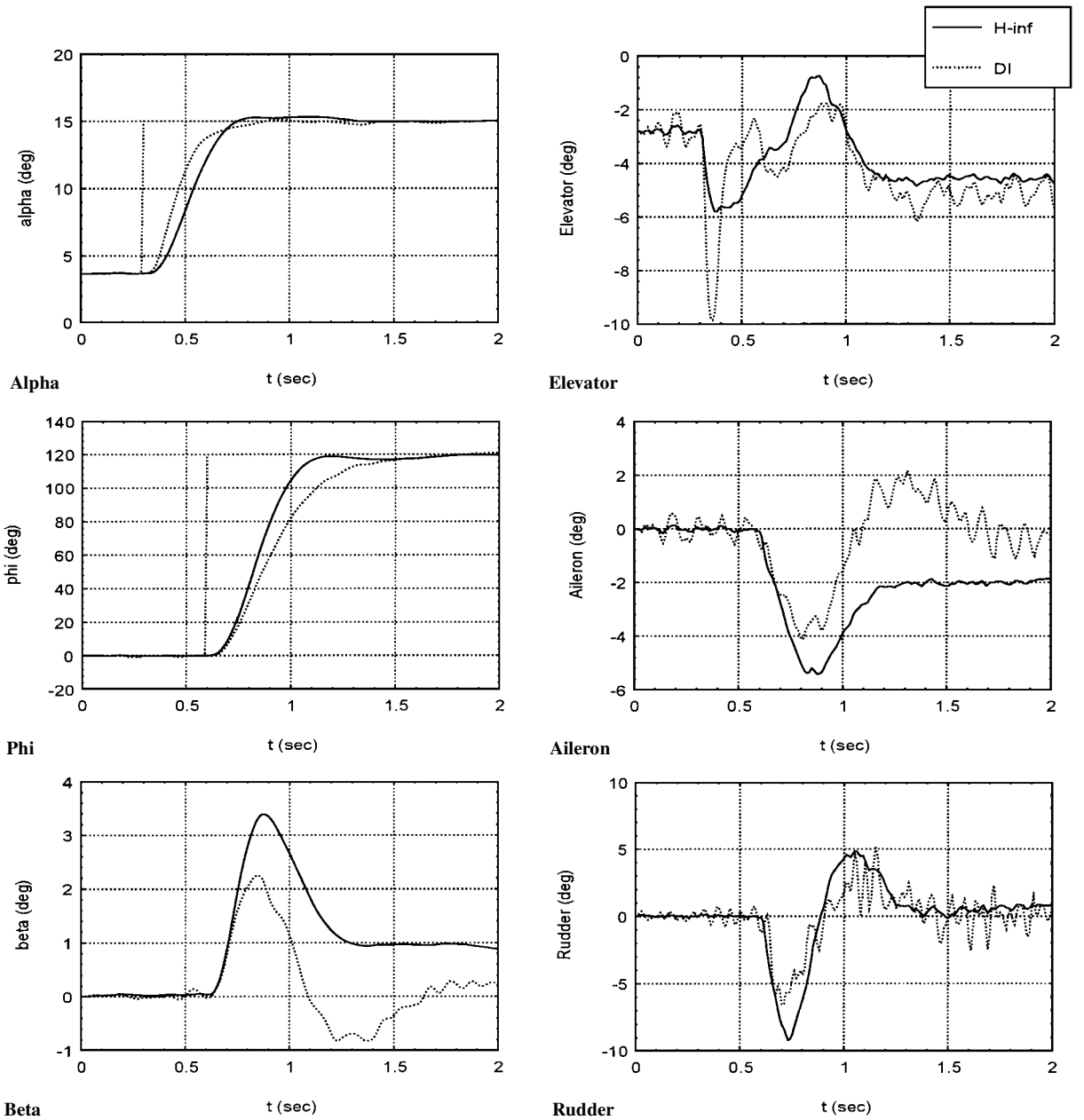

Fig. 10 Dynamic response with noisy measurements: $\mathcal{H}_\infty$ and dynamic inversion controllers.

C. Robustness

Because the values of aerodynamic coefficients may have substantial uncertainties, missile autopilots have to be robust to variations in the aerodynamic coefficients. To test the robustness of the two controller designs, we changed the values of the true coefficients by up to $\pm 20\%$ and simulated a variety of maneuvers. For the dynamic inversion controller, the tabulated values were used to calculate the inversion, whereas the perturbed values were used in the state equations. The state values and control deflections during one such maneuver are shown in Figs. 8 and 9. For that maneuver, the missile starts at $\alpha = 3.66$ deg and $\phi = 0$ deg with a velocity of 2086 ft/s. The missile is given commands of $\alpha_c = 15$ deg and $\phi_c = 120$ deg. The solid lines represent the maneuver done with the nominal dynamics. The dashed lines show the results with the aerodynamic coefficients changed.

For the robustness test, we used a real uncertainty similar to the complex uncertainty that caused instability in the linearized closed-loop system with the dynamic inversion controller. The MatLab mu command can be used to find the smallest destabilizing complex uncertainty for the linear system tested. The complex-μ plot for the dynamic inversion controller was almost identical to the real-μ plot at low frequencies, and the destabilizing uncertainty had a complex component only 0.2 times the size of the real component, so that a similar, real uncertainty was used to test the robustness of the actual nonlinear, closed-loop dynamics. We used 20% real variations in the appropriate coefficients, where the μ-analysis test indicated instability of the linearized dynamics with 16% complex variations in the aerodynamic coefficients. The destabilizing uncertainty given by the μ-analysis test for the linearization was complex, so that this uncertainty is not identical, but it is similar. The simulation results for the robustness test are shown in Fig. 8 for the $\mathcal{H}_\infty$ controller and Fig. 9 for the dynamic inversion controller.

The $\mathcal{H}_\infty$ controller had some losses in tracking performance with this uncertainty. Both the α and ϕ responses exhibited increased overshoot and longer settling times. The maximum sideslip angle reached increased by 60%. The control deflections were similar to those used without the uncertainty. For the dynamic inversion controller, the α response takes over 2 s to settle down to the commanded value. The lateral dynamics are unstable with the chosen aerodynamic uncertainty. The ϕ response overshoots the commanded value and then slowly increases. Sideslip angle slowly increases.

Neither controller was specifically designed to have a certain level of robustness. Robustness to 20% uncertainties in the aerodynamic coefficients was a design goal but was not specifically included in

the design methodology for either controller, giving more insight into the inherent robustness of each method.

D. Noise Rejection

The next step in our comparative study of these two controller designs was to examine their sensitivity to measurement noise. We added noise to the values of α, β, ϕ, p, q, and r used by the controllers. The noise model we used was white noise with a variance of 1% of the mean square values of the corresponding states. Each noise signal was passed through the filter $(0.25s + 1)/(0.025s + 1)$ and then added to the corresponding states for use by the controllers.

The simulation tests were performed with this noise model and the same maneuver used in the robustness tests discussed earlier. The results of the simulation are shown in Fig. 10. These plots clearly show that the dynamic inversion controller is more sensitive to measurement noise than the $\mathcal{H}_\infty$ controller. This is because of the faster controller response and higher crossover frequency of the dynamic inversion controller. The state responses with the dynamic inversion controller are still acceptable, but the noise causes significant high-frequency variation in the controller deflections. This is of particular concern because the crossover frequency of the dynamic inversion controller cannot be easily reduced. We performed simulations where the filters used to guarantee the necessary attenuation of controller deflection commands (see Sec. IV) were adjusted to reduce the crossover frequency, and these tests resulted in instability due to inadequate timescale separation from the inner-loop dynamics.

VI. Conclusions and Suggestions for Future Work

Nonlinear flight control systems were designed for a BTT, air-to-air missile using two different design methodologies. These methodologies, $\mathcal{H}_\infty$ control with $\mathcal{D}$-implementation gain scheduling and dynamic inversion, were compared on a variety of issues, primarily achievable performance, robustness to uncertainty in the aerodynamic coefficients, and noise rejection. A full nonlinear simulation of selected maneuvers was performed with both controllers. Similar response speeds were achieved with both design methods, with the dynamic inversion controller better controlling coupling between the longitudinal and lateral dynamics. Nonlinear simulation results indicated good robustness for the $\mathcal{H}_\infty$ controller. The dynamic inversion controller did not maintain stability of the nonlinear dynamics under certain allowable uncertainties in the aerodynamic coefficients. Using a complex μ-analysis test, we were able to find allowable uncertainties in the aerodynamic coefficients for which the closed-loop system with the dynamic inversion controller was unstable. The $\mathcal{H}_\infty$ controller guarantees a certain level of robustness, at least locally. The dynamic inversion controller was also more sensitive to measurement noise than the $\mathcal{H}_\infty$ controller. Recommendations for future research include a more detailed analysis of the robustness properties of both controller designs, particularly the dynamic inversion design.

Acknowledgment

This work was supported in part by the Air Force Office of Scientific Research under Contract F-49620-93-1-0246DEF.

References

[1]Kaminer, I., Pascoal, A. M., Khargonekar, P. P., and Coleman, E. E., "Velocity Algorithm for the Implementation of Gain-Scheduled Controllers," *Automatica*, Vol. 31, No. 8, 1995, pp. 1185–1191.

[2]Baumann, W. T., and Rugh, W. J., "Feedback Control of Nonlinear Systems by Extended Linearization," *IEEE Transactions on Automatic Control*, Vol. 31, No. 1, 1986, pp. 40–46.

[3]Lawrence, D. A., and Rugh, W. J., "Gain Scheduling Dynamic Linear Controllers for a Nonlinear Plant," *Proceedings of the 32th IEEE Conference on Decision and Control*, Inst. of Electrical and Electronics Engineers, New York, 1993, pp. 1024–1029.

[4]Rugh, W. J., "Analytical Framework for Gain Scheduling," *IEEE Control Systems Magazine*, Vol. 11, No. 1, 1990, pp. 74–84.

[5]Packard, A., "Gain Scheduling via Linear Fractional Transformations," *Systems and Control Letters*, Vol. 22, No. 2, 1994, pp. 79–92.

[6]Shamma, J. S., and Athans, M. A., "Analysis and Design of Gain Scheduled Control Systems," *IEEE Transactions on Automatic Control*, Vol. 35, No. 8, 1990, pp. 898–907.

[7]Stein, G., Hartmann, G., and Hendrick, R., "Adaptive Control Laws for F-8 Flight Test," *IEEE Transactions on Automatic Control*, Vol. 22, 1977, pp. 758–767.

[8]Bugajski, D. J., and Enns, D. F., "Nonlinear Control Law with Application to High Angle-of-Attack Flight," *Journal of Guidance, Control, and Dynamics*, Vol. 15, No. 3, 1992, pp. 761–767.

[9]McFarland, M. B., and D'Souza, C. N., "Missile Flight Control with Dynamic Inversion and Structured Singular Value Synthesis," *Proceedings of the AIAA Guidance, Navigation, and Control Conference* (Scottsdale, AZ), AIAA, Washington, DC, 1994, pp. 544–550.

[10]Snell, S. A., Enns, D. F., and Farrard, W. L., "Nonlinear Inversion Flight Control for a Supermaneuverable Aircraft," *Journal of Guidance, Control, and Dynamics*, Vol. 15, No. 4, 1992, pp. 976–984.

[11]D'Souza, C., and Schumacher, D., "Derivation of the Full Nonlinear Equations of Motion for a Rigid Airframe," *Journal of Guidance, Control, and Dynamics* (to be published).

[12]Blakelock, J. H., *Automatic Control of Aircraft and Missiles*, 2nd ed., Wiley, New York, 1991, Chaps. 1 and 7.

[13]Schumacher, D. A., "Tactical Missile Autopilot Design Using Nonlinear Control," Ph.D. Thesis, Dept. of Aerospace Engineering, Univ. of Michigan, Ann Arbor, MI, 1994.

[14]Carter, L. H., and Shamma, J. S., "Gain-Scheduled Bank-to-Turn Autopilot Design Using Linear Parameter Varying Transformations," *Journal of Guidance, Control, and Dynamics*, Vol. 19, No. 5, 1996, pp. 1056–1063.

[15]Schumacher, C., and Khargonekar, P. P., "Modeling and Control of a Bank-to-Turn Air-to-Air Missile," Dept. of Electrical Engineering and Computer Science, TR CGR97-02, Univ. of Michigan, Ann Arbor, MI, Feb. 1997.

[16]Ruth, M. J., and Arrow, A., "Preliminary Bank-to-Turn Autopilot Study for USAF HaveDash Air-to-Air Missile," Applied Physics Lab., Johns Hopkins Univ., 1989.

[17]Niewoehner, R. J., and Kaminer, I. I., "Design of an AutoLand Controller for an F-14 Aircraft Using $\mathcal{H}_\infty$ Synthesis," *Journal of Guidance, Control, and Dynamics*, Vol. 19, No. 3, 1996, pp. 656–663.